

Article

Tunable Adhesion of Shape Memory Polymer Dry Adhesive Soft Robotic Gripper via Stiffness Control [†]

ChangHee Son ¹ , Subin Jeong ², Sangyeop Lee ², Placid M. Ferreira ¹ and Seok Kim ^{1,2,3,*}

¹ Department of Mechanical Science and Engineering, University of Illinois at Urbana-Champaign, Urbana, IL 61801, USA; cs21@illinois.edu (C.S.); pferreir@illinois.edu (P.M.F.)

² Department of Mechanical Engineering, Pohang University of Science and Technology, Pohang 37673, Republic of Korea; sooibing@postech.ac.kr (S.J.); sylee7361@postech.ac.kr (S.L.)

³ Institute for Convergence Research and Education in Advanced Technology, Yonsei University, Seoul 03722, Republic of Korea

* Correspondence: seok.kim@postech.ac.kr

[†] This is paper is an extended version of our paper published in Son, C.; Kim, S. A Shape Memory Polymer Adhesive Gripper For Pick-and-Place Applications. In Proceedings of the 2020 IEEE International Conference on Robotics and Automation (ICRA), Paris, France, 31 May 2020–31 August 2020; pp. 10010–10016.

Abstract: A shape memory polymer (SMP) has been intensively researched in terms of its exceptional reversible dry adhesive characteristics and related smart adhesive applications over the last decade. However, its unique adhesive properties have rarely been taken into account for other potential applications, such as robotic pick-and-place, which might otherwise improve robotic manipulation and contribute to the related fields. This work explores the use of an SMP to design an adhesive gripper that picks and places a target solid object employing the reversible dry adhesion of an SMP. The numerical and experimental results reveal that an ideal compositional and topological SMP adhesive design can significantly improve its adhesion strength and reversibility, leading to a strong grip force and a minimal release force. Next, a radially averaged power spectrum density (RAPSD) analysis proves that active heating and cooling with a thermoelectric Peltier module (TEC) substantially enhances the conformal adhesive contact of an SMP. Based on these findings, an adhesive gripper is designed, fabricated, and tested. Remarkably, the SMP adhesive gripper interacts not only with flat and smooth dry surfaces, but also moderately rough and even wet surfaces for pick-and-place, showing high adhesion strength (>2 standard atmospheres) which is comparable to or exceeds those of other single-surface contact grippers, such as vacuum, electromagnetic, electroadhesion, and gecko grippers. Lastly, the versatility and utility of the SMP adhesive gripper are highlighted through diverse pick-and-place demonstrations. Associated studies on physical mechanisms, SMP adhesive mechanics, and thermal conditions are also presented.

Keywords: dry adhesives; shape conformation; shape memory polymer; robotic soft gripper



Citation: Son, C.; Jeong, S.; Lee, S.; Ferreira, P.M.; Kim, S. Tunable Adhesion of Shape Memory Polymer Dry Adhesive Soft Robotic Gripper via Stiffness Control. *Robotics* **2023**, *12*, 59. <https://doi.org/10.3390/robotics12020059>

Academic Editor: Gursel Alici

Received: 10 March 2023

Revised: 7 April 2023

Accepted: 7 April 2023

Published: 17 April 2023



Copyright: © 2023 by the authors. Licensee MDPI, Basel, Switzerland. This article is an open access article distributed under the terms and conditions of the Creative Commons Attribution (CC BY) license (<https://creativecommons.org/licenses/by/4.0/>).

1. Introduction

Robotic grippers have been extensively researched for a variety of applications in diverse fields to overcome the limitations of human capabilities. The manufacturing or logistics industry uses the grippers because they can lift heavy objects or do repetitive manipulation, which lessens the burden on human workers [1,2]. The aerospace industry requires a robotic gripper for outer space which is gravity-independent, freezing, and lacks air [3,4]. Food industries extensively utilize robotic grippers for food processing, cooking, and packaging [5–8]. Robotic grippers are also being developed for use in surgery and rehabilitation in the medical industry [9,10]. Underwater grippers have been researched to investigate oceanographic samples [11,12]. Microassembly with grippers has allowed for the creation of unique three-dimensional microelectromechanical systems (MEMS) that are not possible with other methods [13–15].

Various robotic gripper systems have been introduced to meet the aforementioned demands. Traditional finger grippers containing rigid links and joints are simple yet effective. However, these grippers are often inadequate for picking target objects with challenging shapes and properties. Those objects may be too large, have only a single surface for picking such as plates, be too soft and deformable, or require a sophisticated feedback control to avoid damaging objects that are fragile or brittle [16,17]. Soft grippers have been widely studied to overcome these challenges [18,19]. Soft finger grippers can passively adapt to the target object and provide additional stability for grasping [20]. Fluid-actuated elastomer grippers can generate high forces depending on the applied pressure of the fluid [21]. However, both soft finger and fluid-actuated grippers still have the common drawback that the target objects they lift must have multiple surfaces with acceptable dimensions to be gripped. If lifting objects are formed of ferrous materials, electromagnetic grippers have the advantage of easy and quick lifting and releasing [22], which is also their inherent limitation in terms of material choice. Grippers with dielectric elastomer actuators are very flexible and can obtain high strain with relatively low stress [23–25]. Vacuum grippers can lift heavy things and can even be utilized to climb walls [26,27]. They would not, however, work in a vacuum or on porous surfaces. Because of their quick response time, electroadhesion grippers based on electrostatic force are also useful for quick pick-and-place [28]. Nonetheless, the applied voltage must often be very high to achieve strong electroadhesion, which is prone to harming electronic components on sticking surfaces. Gecko grippers do not require an atmosphere to function in space [3] and stick to a variety of surfaces [29–31]. Those grippers seem promising, but they show relatively low adhesive strength, only work on dry surfaces, and are somewhat difficult to manufacture or operate, which may limit their applications. Furthermore, multi-strategy soft grippers have also been studied to accommodate different challenges, such as gecko-adhesion with fluidic actuation [32,33], gecko-adhesion with microspine [34], and vacuum suction with fluidic actuation [35].

Shape memory materials, such as shape memory alloy (SMA) and shape memory polymer (SMP), can also be exploited to design a gripper due to the shape memory effect and their stiffness change through the phase transition. SMPs can inherently adapt to more strain, are less stiff, cheaper, and have more flexibility on transition temperature compared to SMAs. Nevertheless, recent research outcomes on both SMAs and SMPs are mostly concentrated on grasping instead of adhering [36–40]. Some of the SMP grippers that are designed for grasping use external stimuli other than heat, such as light or humidity [41–43]. A more recent SMP gripper picks up the target object by embedding it into SMPs where the friction and suction effects take a majority role [44], which is similar to that of granular jamming grippers [12,45,46] or a tendon-driven self-adaptive gripper [47].

In this work, a more sophisticated SMP dry adhesive gripper based on pure Van der Waals force on an adhesive contact area is presented, and its strong, material-independent, and reversible adhesion is demonstrated for picking flat, smooth, or moderately rough objects. [48] Furthermore, because an SMP's dry adhesion is water-resistant, the SMP adhesive gripper can be used on wet or submerged objects [49]. A thermoresponsive SMP is used here, and it has the ability to stably fix to its deformed or 'temporary' shape when heated, deformed, and cooled. From this temporary shape, the SMP can fully recover its original or 'permanent' shape after being reheated over the glass transition temperature (T_g). This thermoresponsive SMP, in particular, experiences a significant shift in storage modulus across the T_g between glassy and rubbery states and generally exhibits a strong shape memory effect when subjected to thermomechanical loading [49–52]. Within the context of the dry adhesive properties, the SMP becomes soft in its rubbery state when heated and establishes a conformal and hermetic contact with a dry or wet opposing surface once the pressure is applied. The SMP becomes rigid in its glassy state after being cooled with pressure, yet it maintains contact with the opposing surface, forming a strong dry adhesion. However, the SMP tends to lose its strong adhesive contact when reheated, resulting in reversible dry adhesion.

The storage moduli of the SMPs used in this study as a function of temperature and their employment as an adhesive hook are shown in Figure 1. These storage moduli are determined using the TA instrument Q800 Dynamic Mechanical Analysis. We first present the method to fabricate the SMP adhesives and the adhesion force measurement procedure in Section 2. The mechanics at the adhesive interface upon compositional and topological variations of the SMP adhesive are introduced in Section 3. The concept of a bi-layer SMP more favorable to absorbing dynamic stress, high shock, and energy is shown in Section 4, which is similar to the concept of viscoelastic adhesives proven in prior work [53–55]. In Section 5, the thermoelectric Peltier module (TEC) is implemented into the SMP adhesives to function as both heater and cooler. The TEC not only reduces the overall operation time but also enhances the adhesion strength. The adhesion improvement here is achieved from improved surface contact conformability in surface roughness scale which is validated by comparing radially averaged power spectral density (RAPSD) of the SMP and target adherend surface roughness profiles. Finally, the performance of the SMP adhesive gripper on various surfaces along with its picking and placing mechanisms and temperature profiles is demonstrated in Section 6. It is worthwhile to note that this work is extended from the previous conference work [45] and includes substantial additional results with research significance.

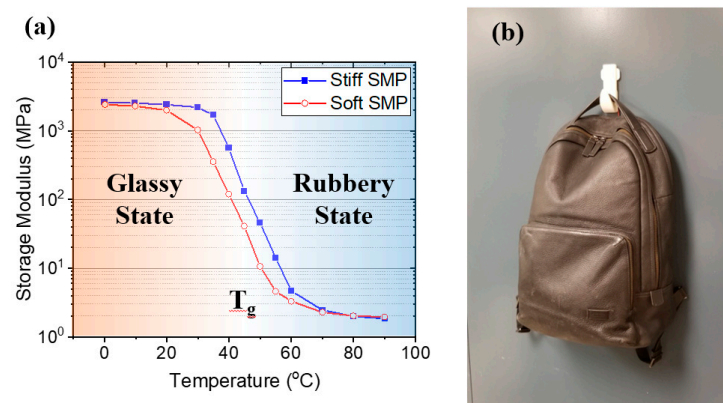


Figure 1. (a) Temperature dependence of the storage moduli of stiff and soft shape memory polymers (SMPs); (b) a reversible dry adhesive hook employing the SMP.

2. Methods

2.1. Fabrication of the SMP

The SMP utilized in this study is created using a process that was developed elsewhere [50]. First, a 110 °C oven is used to preheat Poly(Bisphenol A-co-epichlorohydrin), glycidyl end-capped with a molecular weight of 1075 g/mol from Sigma-Aldrich (St. Louis, MO, USA), hereafter called E1075, and diglycidyl ether of bisphenol A epoxy monomer with a molecular weight of 362 g/mol from Momentive, hereafter called EPON 826. E1075 and EPON 826 are thoroughly mixed to form the epoxy monomer when they have fully melted. The epoxy monomer is then combined with a curing agent, Jeffamine D-230, poly(propylene glycol)bis(2-aminopropyl) ether (Huntsman), hereafter called Jeffamine, which has an average molecular weight of 230 g/mol. The weight-based mixing ratio of E1075, EPON 826, and Jeffamine is 0.940:1.000:0.837 for the stiff SMP and 0.334:1.000:0.707 for the soft SMP. The resultant SMP precursor is poured onto a 3 × 2 inch glass slide wrapped with PTFE tape (Tapecase), and air bubbles are extracted using a pipette. Curing requires 120 min heating on a hot plate at 80 °C. The SMP is readily peeled off the PTFE tape in either its rubbery or glassy state after it has fully cured.

2.2. Adhesion Test Setup

Figure 2 depicts the test setup to measure the adhesion strength of SMP samples. A fishing line connects the backing aluminum block with an SMP to a bucket through the

pulleys. A cartridge heater and a thermocouple are located inside the aluminum block and are connected to a temperature controller. To measure the maximal adhesion strength of the SMP, it is heated to above 80 °C to its rubbery state. Then, to make conformal adhesive contact with the target plate, a preload of 4.54 kg (0.895 atm) is applied to the SMP. The heater is turned off, and the SMP is cooled without removing the preload. The SMP transforms into a glassy state after cooling down to 30 °C. Then, water is slowly pumped into the bucket until the adhesive contact fails to measure the maximum adhesion of the glassy state SMP. Otherwise, the SMP is reheated to above 80 °C, and water is pumped to obtain the minimal adhesion of the rubbery state SMP. For adhesion strength over 2.5 atm, additional weight is placed in the bucket before pumping in water because the full bucket of water does not cause adhesive contact failure. When the SMP detaches from the target plate, the weight of water, additional weight, and the bucket is measured to determine either the maximum or minimal adhesion strength.

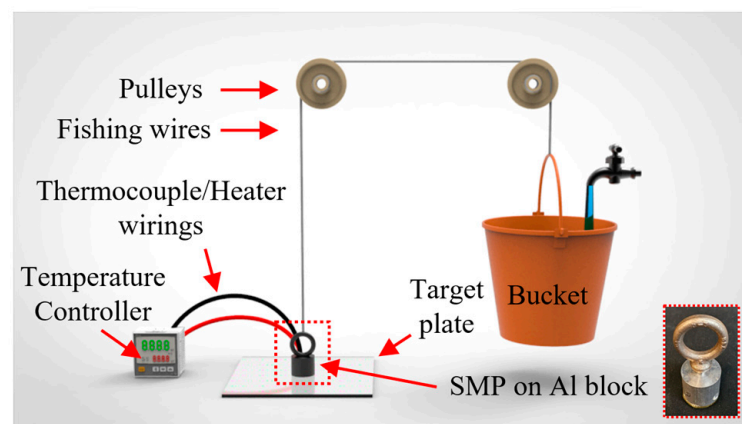


Figure 2. A test setup to measure the adhesion strength of an SMP sample. While an SMP adheres to the target plate, the bucket is filled with water. The adhesion strength of the SMP is measured once it fails to adhere to the target plate.

3. Dual SMP and Release Tip SMP

3.1. Fabrication of Dual SMP and Release Tip SMP

Single, dual, and release tip SMP samples are prepared in different ways as shown in Figure 3, and the adhesion strengths of these SMP samples are quantitatively evaluated in response to compositional and topological design modifications. First, a single SMP sample is fabricated from cured stiff SMP that is cut into a 25 mm diameter round form using an Epilog Laser Fusion M2 laser cutter (Figure 3a). The other single SMP can also be made of a cured soft SMP in the same way. For a dual SMP sample, a cured soft SMP is sliced into a 5 mm width and 25 mm outer diameter ring form using a laser cutter. The middle hollow portion is then filled with a stiff SMP precursor and cured (Figure 3b). Finally, using Loctite Instant Mix epoxy, the completed SMP sample is bonded to a backing aluminum block. Here, the rigid backing aluminum block helps uniformly distribute strain and provides spaces for the cartridge heater, thermocouple, and hook. The last type of SMP sample is to minimize the force required to release the SMP at the rubbery state by having a release tip on an SMP surface. This release tip SMP is fabricated by curing a single drop of stiff SMP precursor that is applied with a pipette on a cured 25 mm diameter stiff SMP. The release tip is located 8.5 mm away from the center, with a radius of 5.08 mm and a maximum height of 0.64 mm, as shown in Figure 3c.

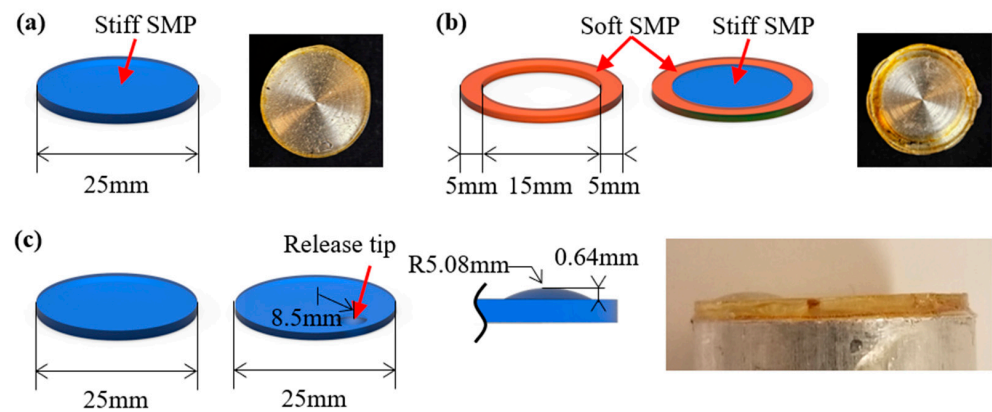


Figure 3. (a) The fabrication of a single SMP sample. A 25 mm diameter circular form is carved out of a cured thick SMP; (b) the fabrication of a dual SMP sample; after curing and cutting a soft SMP into a ring form, a stiff SMP precursor is filled and cured inside the ring-shaped soft SMP; (c) the fabrication of a release tip SMP sample; a single drop of SMP precursor is deposited on the SMP surface and cured to form a release tip on a 25 mm diameter SMP sample.

3.2. Numerical Results of Dual SMP and Release Tip SMP

A finite element analysis (FEA) on the first principal stress is used to investigate the effect of SMP stiffness and composition on adhesion. The boundary condition is shown in the inset image in Figure 4a where the displacement is restricted at the SMP bottom surface, which is in contact with a target plate, and the external force is applied to the aluminum block’s top surface. Young’s modulus is chosen as 2000 MPa for the stiff SMP and 1000 MPa for the soft SMP, assuming that the SMPs are in their glassy state at 30 °C, as deduced from the data in Figure 1a. The resultant first principal stress at the bottom surface along the A–A’ line of the SMP is illustrated. Both single soft and stiff SMPs exhibit significantly high stress concentration near the SMP’s edge. The dual SMP result, on the other hand, reveals that stress is more evenly transferred to the center, which helps lessen the stress concentration at the outer edges. Therefore, a contact failure commencing at the outer edge would occur by a higher external load as a result of the lowered stress concentration at the outer edge. This implies that the dual SMP should have a larger maximum adhesion strength than both single soft and stiff SMPs, which is in line with the findings of prior work [56].

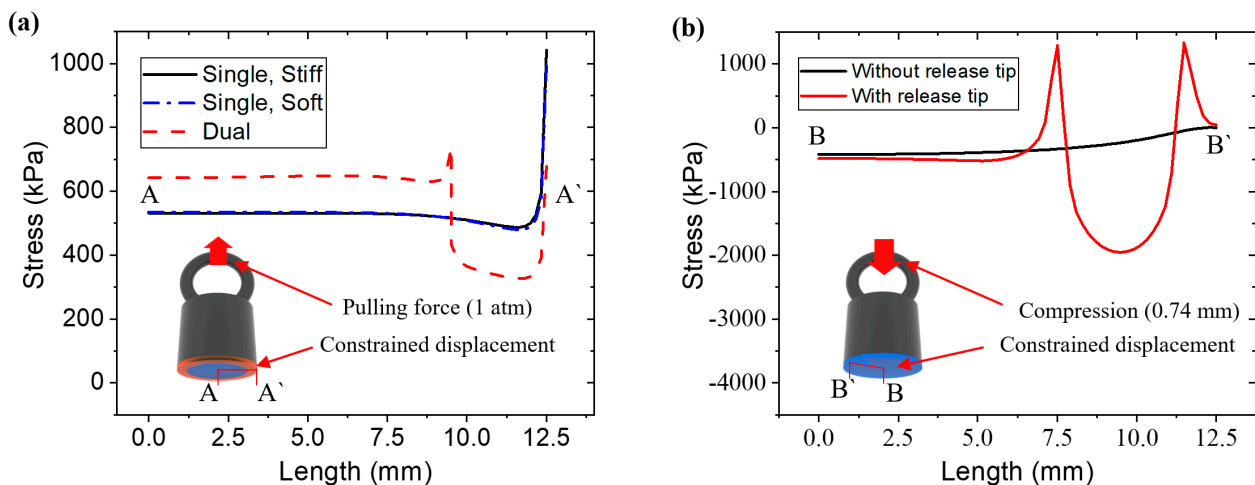


Figure 4. (a) The schematic dual SMP sample attached to the aluminum block with its boundary condition and the FEA plot of the first principal stress along the A–A’ line; (b) the schematic SMP with a release tip attached to the aluminum block with the boundary condition and the FEA plot of the first principal stress along the B–B’ line.

Moreover, the minimal adhesion strength of the rubbery SMP with and without a release tip is compared via numerical analysis. The inset illustration in Figure 4b depicts the boundary condition where a prescribed displacement of 0.74 mm is applied downwards towards the target plate that is fixed. This quantity is chosen to compress the release tip completely ($0.64 \mu\text{m}$ thick), which can be proved from the FEA, while also providing $0.1 \mu\text{m}$ of additional compression to the rest of the SMP. Young's modulus is set to 20 MPa which is the modulus of the SMP in the rubbery state at 80°C . The resultant first principal stress along the B–B' line at the bottom surface of the SMP is presented. The compressive stress increases towards the center of the SMP sample without the release tip. The release tip SMP sample, in contrast, shows a dramatical stress concentration near the release tip which consists of both tensile and compressive components. As a result, when the prescribed displacement is removed while the SMP is still rubbery, the release tip SMP tends to pop up and may self-peel due to the high stress concentration around the release tip. However, in the glassy state of the SMP, the release tip can be fixed in a collapsed shape and still exhibit a decent adhesion. Consequently, adding a release tip to the SMP reduces the rubbery state SMP's minimum adhesion and may permit self-peeling without compromising its maximum adhesion in the glassy state significantly.

3.3. Experimental Results of Dual SMP and Release Tip SMP

The experimental adhesion strength measurement quantifies the qualitative prediction of higher maximum adhesion strength and reversibility (the ratio between maximum and minimum adhesion strength) with dual SMP and release tip SMP designs. In Figure 5a, the maximum adhesion strength of single and dual SMPs is evaluated using the test setup shown in Figure 2. The average adhesion strength for single soft SMP, single stiff SMP, and dual SMP are 1.75 atm, 2.28 atm, and 4.83 atm, respectively, after 3 tests per individual sample. The stiff SMP exhibits higher adhesion than the soft SMP although the stress concentration for both soft and stiff SMPs is nearly identical, as shown in Figure 4a. When the same load is given to both soft and stiff SMPs, the soft SMP accumulates more strain energy, making it more susceptible to contact failure. As a result, the soft SMP's maximum adhesion strength is lower than that of the stiff SMP as evaluated experimentally. More crucially, the dual SMP's maximal adhesion strength is more than twice that of single SMPs. The edge of single SMPs is particularly sensitive to contact failure due to high stress concentration. However, as predicted by the numerical results, the dual SMP distributes stress more uniformly from edge to center, resulting in a significant increase in maximum adhesion strength.

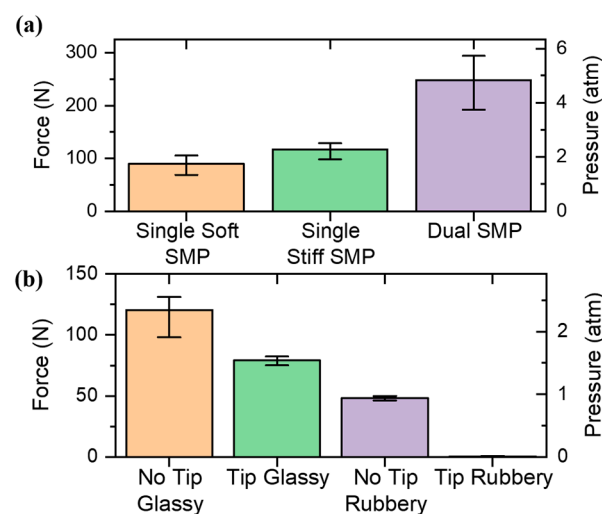


Figure 5. (a) The maximal adhesion strength of single and dual SMPs, as tested experimentally; (b) adhesion strength of SMPs with and without release tip in glassy and rubbery states, as evaluated experimentally; the error bar represents the maximum and minimum of the three tested results.

Figure 5b illustrates the maximum and minimum adhesion strength of SMPs with and without a release tip which is experimentally measured using the test setup in Figure 2. When a release tip is added, the maximum adhesion strength at the glassy state drops from 2.35 atm to 1.54 atm. However, the minimum adhesion strength, which is the force needed to peel off the SMP in its rubbery state, drops drastically from 0.936 atm to 0.00955 atm when a release tip is introduced. The rubbery state release tip SMP can be assumed to show self-peeling because the peeling force is almost non-existent. Even though the release tip sacrifices 34% of the glassy SMP's maximum adhesion strength, the SMP's self-peeling should be encouraged since it is highly useful in real-world applications.

4. Bi-Layer SMP

4.1. Fabrication of Bi-Layer SMP

To analyze the enhanced work of adhesion stemming from the bi-layer design [53–55], a bi-layer SMP sample is fabricated as shown in Figure 6. First, the soft SMP layer of 0.5 mm thickness is cured on a glass slide following the method introduced in Section 2. Next, a 2 mm thick layer of the stiff SMP precursor is poured over the soft SMP and cured. The fully cured bi-layer SMP is ready to be cut into any shape using a preprogrammed laser cutter. Here, the bi-layer SMP sample is cut into a 25 mm diameter round form and fixed on a backing aluminum block using Loctite Instant Mix epoxy for adhesion testing. Here, a 2.5 mm thick single-layer stiff SMP is also prepared as a control sample.

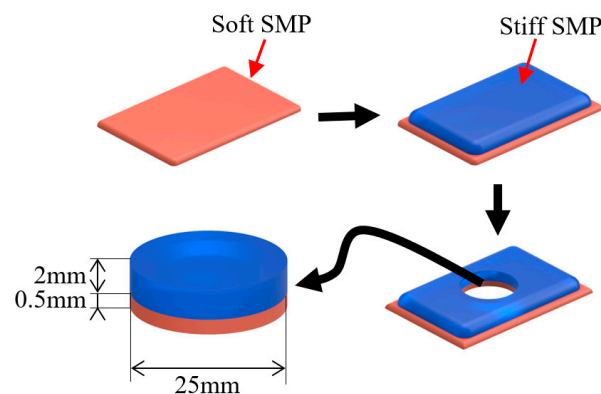


Figure 6. The fabrication of a bi-layer SMP sample. A 0.5 mm thick soft SMP is cured on a glass slide. Then, 2 mm thick stiff SMP is cured on top of the soft SMP. After being fully cured, the bi-layer SMP is cut using a laser cutter in a 25 mm diameter circular form.

4.2. Experimental Results of Bi-Layer SMP

The adhesion of the bi-layer SMP is tested using the tensile tester (Instron universal testing system) instead of the setup in Figure 2 to quantify the resultant force-displacement curves. First, the compression platens are installed to the tester, and the adherend is fixed on a lower platen. The SMP is heated over 80 °C using the cartridge heater installed in the backing aluminum block, and about 2 atm preload is applied by pressing down the flat surface of the upper compression platen. Once the SMP is cooled back down to 30 °C, the upper compression platen is removed and only the clevis pin is left. A hook is installed on an aluminum backing block, and the hook is connected with the clevis pin using fishing wires.

A pretension of 5 N is given to stretch and make the wires tight. Then, the SMP is pulled off from the adherend surface at a 4 mm/min constant rate. Figure 7 shows the resultant data of the normal force and the displacement that are measured every 0.1 s. Here, the work of adhesion is calculated from (1).

$$W = \int_0^{d_{max}} \frac{F(\delta)}{A} d\delta \quad (1)$$

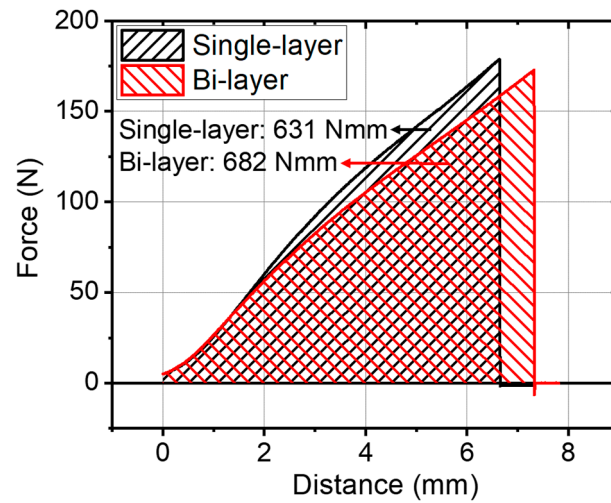


Figure 7. The force-distance curves for SMP samples. The areas under the curves, which indicate the work for the single-layer SMP and bi-layer SMP, are 631 Nmm and 682 Nmm, respectively.

The work of adhesion and peak adhesion strength are 1.29 mJ/mm² and 179 N for the single-layer SMP, and 1.39 mJ/mm² and 173 N for the bi-layer SMP. The data show that implementing the bi-layer design can increase the work of adhesion by 8% but sacrifices the peak adhesion strength by 3.35%. The results prove that the bi-layer SMP design is superior to a single-layer SMP in terms of work of adhesion and thus more favorable to absorbing high shock, energy, and dynamic stress.

5. Thermoelectric Peltier Module

5.1. Schematics of Thermoelectric Peltier Module

Controlling the temperature of the SMP is also critical in determining the adhesion strength of the SMP in addition to the foregoing compositional and topological factors. Depending on the thermal characteristics of the adherend, a rubbery SMP may suddenly experience low temperature at the contact interface at the time of contact and shift into the glassy state, which hinders the SMP from making ideal conformal contact. As shown in Figure 8, a 12V thermoelectric Peltier module TEC1-12710, hereafter TEC, is utilized to control both heating and cooling. Here, a commercial central processing unit (CPU) cooler is also used to reduce the heat that is created due to the exothermic nature of the TEC.

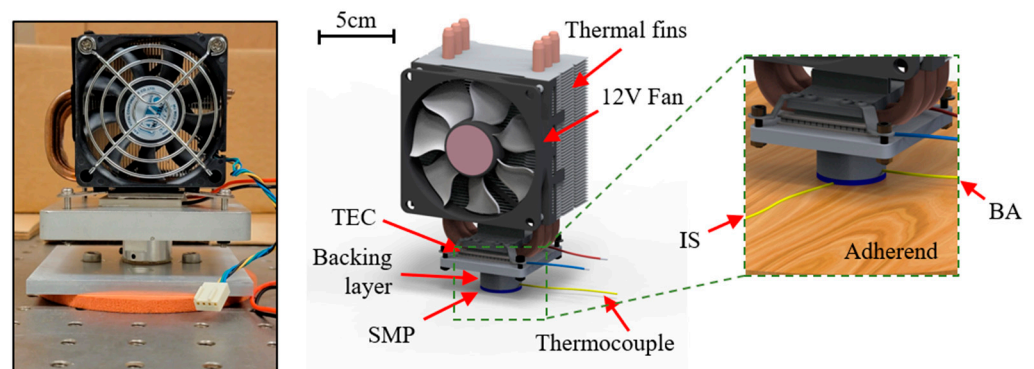


Figure 8. The schematic of a test setup with a thermoelectric Peltier module (TEC) for measuring the adhesion force at failure and the temperature at the center of a backing aluminum (BA) and at the interface between the SMP and the adherend (CI).

A thermocouple is inserted into a side drill hole of the backing aluminum close to the SMP layer, and it reaches the center of the cylinder shaped backing aluminum (BA) to measure the temperature. Similarly, the temperature of the SMP–adherend contact interface

(CI) is also measured to check the temperature deviation between BA and CI. While only BA temperature is monitored when adhesion strength is measured in Figure 9, both BA and CI temperature values are monitored when drawing the temperature profiles in Figure 10.

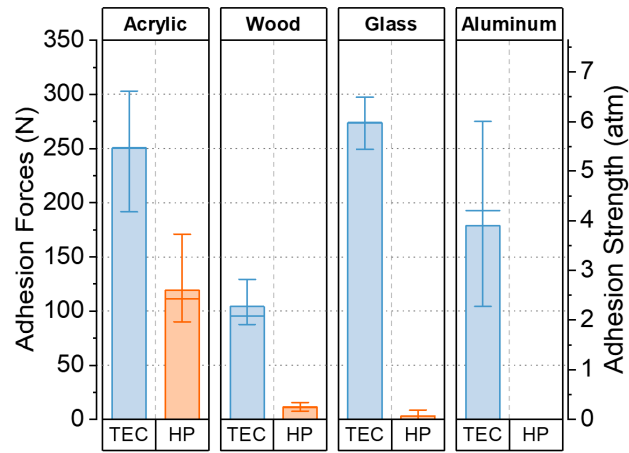


Figure 9. The adhesion force that is formed using a thermoelectric module (TEC) and a hotplate (HP) as heating methods for four different adherend materials which are acrylic, wood, glass, and aluminum. The three lines of the error bar represent the maximum, median, and minimum values, respectively, from top to bottom.

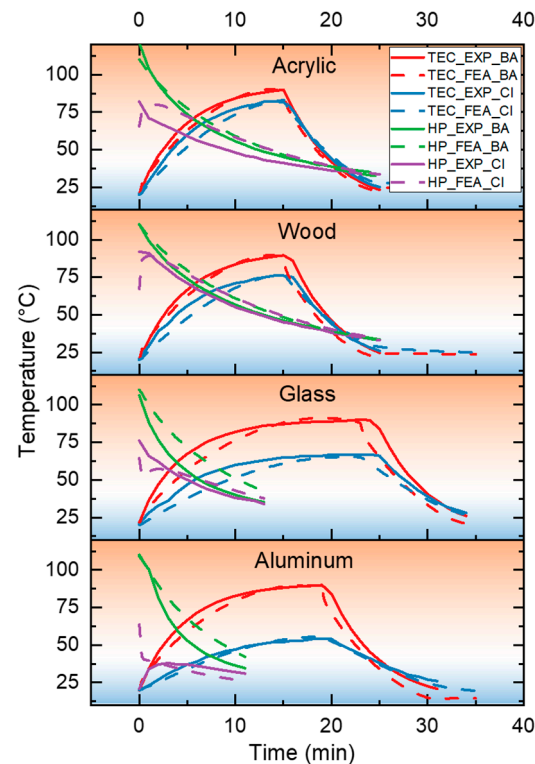


Figure 10. The temperature profiles at the center of the backing aluminum (BA) and at the interface between the SMP and the adherend (CI). The solid lines indicate the experimental results (EXP), and the dashed lines represent the finite element analysis results (FEA). Two different cases are tested: one using the thermoelectric module (TEC) for both heating and cooling, and another using only a hotplate as a heating method (HP). Four plots show the results from different adherend materials which are acrylic, wood, glass, and aluminum. The background of each plot is a gradient filled with colors based on the state of the SMP (rubbery or glassy state).

5.2. Adhesion Strength and Temperature Profile

To create the adhesive contact using TEC, BA is heated to 90 °C, while the 1 atm preload is applied. Once it reaches 90 °C, TEC is switched to the cooling mode by reversing the current direction. After the BA cools down to 25 °C, the TEC is removed, leaving just the cylindrical aluminum block. Then, the adhesion strength is tested as shown in Figure 2.

As a comparison, the adhesion strength after heating the SMP using a hotplate (HP) is also measured. This method creates the adhesive contact of the SMP by heating the aluminum block directly on a hotplate until the BA reaches 110 °C and then cooled to 25 °C with natural convective cooling while a 1 atm preload is applied. Then, as shown in Figure 2, the adhesion strength is measured.

The resulting experimental adhesion strength measurement data are shown in Figure 9. The bar represents the mean value of five test results. The three lines of the error bar represent the maximum, median, and minimum values, respectively, from top to bottom. Here, four different adherend materials are used, and those are acrylic, wood, glass, and aluminum. While other factors can affect the adhesion strength, here we focus on two critical adherend properties which are thermal conductivity and surface roughness of the adherend as listed in Table 1. Generally, when the surface is rough, a flat SMP does not create a good conformal contact which leads to failure at lower adhesion strength, while smooth adherend surfaces are easy to make a conformal contact. Moreover, when the adherend is thermally conductive, the SMP's CI temperature experiences a sudden drop when the SMP makes a contact with the target adherend. This makes the SMP stiffer; thus, it is more difficult to make a conformal contact. However, the SMP is still able to make a decent adhesion even with the low thermal conductivity adherend if the adherend surface roughness is small. When using HP as a heating method, the acrylic surface shows a satisfactory average adhesion strength of 2.6 atm. However, the wood and glass surfaces with HP have adhesion near 0, and the adhesion does not exist on the aluminum surface. This is because the acrylic surface has both small roughness and low thermal conductivity, while others have either large surface roughness or high thermal conductivity.

Table 1. Material properties for adherends.

Material	Thermal Conductivity ($\frac{W}{mK}$)	Surface Roughness S_a (μm)
Acrylic	0.18	0.327
Wood	0.1	7.52
Glass	1.38	0.266
Aluminum	237	1.49

On the other hand, the adhesion strength significantly increases for all four adherends when using TEC. Moreover, the adherend's thermal conductivity does not critically affect the adhesion strength in comparison to HP counterparts, and only the surface roughness shows a positive correlation with the adhesion strength. The main reason for this effect is that the TEC can recover the heat loss that occurs at the contact interface between the SMP and the adherend. This is supported by the results in Figure 10, where the temperature profiles of the experimental (EXP) and finite element simulation (FEA) results for two locations, CI and BA, are shown. For HP tests, it can be observed that the CI temperature can be maintained over T_g for a while and keeps the SMP in the rubbery state in the case of acrylic, wood, and glass. On the contrary, for aluminum, the CI temperature of the SMP drops below T_g immediately, which means the SMP does not have enough time to make a conformal contact with the adherend. This sudden CI temperature drop can be overcome by actively heating using TEC. The CI temperature on aluminum rises over 50 °C, which is just over the T_g to form a conformal contact. Nonetheless, the storage modulus of the SMP is not as small as that of SMPs at 60 °C or higher. Therefore, the adhesion strength of aluminum did not reach as high as those for glass and acrylic adherends. Lastly, when

the CI temperature is maintained high enough to make a conformal contact using TEC, the adhesion strength is inversely proportional to surface roughness.

5.3. Radially Averaged Power Spectral Density for Surface Profiles

The radially averaged power spectral density (RAPSD) for surface profiles is used to check the shape conformability of the SMP. First, a three-dimensional (3D) surface profile $f(x, y)$ is measured using a Keyence VK-X1000 3D laser scanning confocal microscope, where $f(x, y)$ is discrete data that have a pixel resolution of $M \times N$. Here, x or y has a range of,

$$\begin{cases} x = 0, 1, \dots, M - 1 \\ y = 0, 1, \dots, N - 1 \end{cases} \quad (2)$$

These 3D data are converted into a frequency domain with a two-dimensional (2D) discrete Fourier transform (DFT) to analyze the power of different sizes of wavelengths. This 2D DFT can be represented as,

$$F(u, v) = \sum_{x=0}^{M-1} \sum_{y=0}^{N-1} f(x, y) e^{-2\pi j(\frac{ux}{M} + \frac{vy}{N})} \quad \forall \begin{cases} u = 0, 1, \dots, M - 1 \\ v = 0, 1, \dots, N - 1 \end{cases} \quad (3)$$

Here, since $F(u, v)$ is periodic with a period of $[M, N]$, we can shift the data to place the zero-frequency component at the center of the spectrum [57].

$$G(\hat{u}, \hat{v}) = \begin{cases} F(\hat{u}, \hat{v}) & (0 \leq \hat{u} < \frac{M}{2}, 0 \leq \hat{v} < \frac{N}{2}) \\ F(\hat{u}, \hat{v} + N) & (0 \leq \hat{u} < \frac{M}{2}, -\frac{N}{2} \leq \hat{v} < 0) \\ F(\hat{u} + M, \hat{v} + N) & (-\frac{M}{2} \leq \hat{u} < 0, -\frac{N}{2} \leq \hat{v} < 0) \\ F(\hat{u} + M, \hat{v}) & (-\frac{M}{2} \leq \hat{u} < 0, 0 \leq \hat{v} < \frac{N}{2}) \end{cases} \quad (4)$$

$$\forall \begin{cases} \hat{u} \in \left\{ \hat{u} \mid \left(-\frac{M}{2} \leq \hat{u} < \frac{M}{2}\right) \cup (\hat{u} \in \mathbb{Z}) \right\} \\ \hat{v} \in \left\{ \hat{v} \mid \left(-\frac{N}{2} \leq \hat{v} < \frac{N}{2}\right) \cup (\hat{v} \in \mathbb{Z}) \right\} \end{cases}$$

The resulting values are then normalized as,

$$H(\hat{u}, \hat{v}) = \left(\frac{|G(\hat{u}, \hat{v})|}{M \cdot N} \right)^2 \quad (5)$$

The Cartesian coordinates are now converted into polar coordinates such that $\hat{u} = \rho \cos \psi$, $\hat{v} = \rho \sin \psi$. Here, we floor all ρ to the nearest integer and group the components with the same ρ together such that,

$$W_\rho = \left\{ (\hat{u}, \hat{v}) \mid \rho \leq \sqrt{\hat{u}^2 + \hat{v}^2} < \rho + 1 \right\} = \left\{ \vec{w}_{\rho 1}, \vec{w}_{\rho 2}, \dots, \vec{w}_{\rho k_\rho} \right\} \quad (6)$$

Here, $k_\rho = n(W_\rho)$. The RAPSD can be evaluated by averaging the normalized 2D DFT values for all floored radii ρ ,

$$P(\rho) = \frac{1}{k_\rho} \sum_{n=1}^{k_\rho} H(\vec{w}_{\rho n}) \quad (7)$$

Finally, the resulting $P(\rho)$ is plotted as a function of $Wavelength = \frac{\text{distance between adjacent pixels} \times \max(M, N)}{2\rho}$. The calculation is performed through MATLAB, and the plots are shown in Figure 11. Each plot for Figure 11a–d contains the RAPSD lines for each adherend surface, the flat-state SMP, and the SMP that has previously adhered to the target adherend using the TEC and HP. The individual four plots represent four

different adherend materials, which are acrylic, wood, glass, and aluminum, respectively. The black RAPSD line for the aluminum in Figure 11d has a lot of local peaks, especially in hundreds of μm wavelengths. The green RAPSD line for the flat SMP is a straighter line compared to the aluminum case. Both red and blue RAPSD lines for the SMP surface that is detached from the aluminum surface after it creates a conformal adhesive contact show local peaks resembling the line for the aluminum with some amount of power matching. However, the SMP heated with HP does not follow the line for the aluminum as much as the SMP heated with TEC does. The same effect has been exhibited for all other adherend surfaces despite different roughness values of adherend surfaces. Smoother surfaces, such as glass and acrylic, have less power, and rougher surfaces, such as wood, have more power than the flat SMP. These four plots clearly show that SMPs heated with TEC make improved conformal contact with target adherends, thus creating higher adhesion strength than HP-heated SMPs as shown in Figure 9.

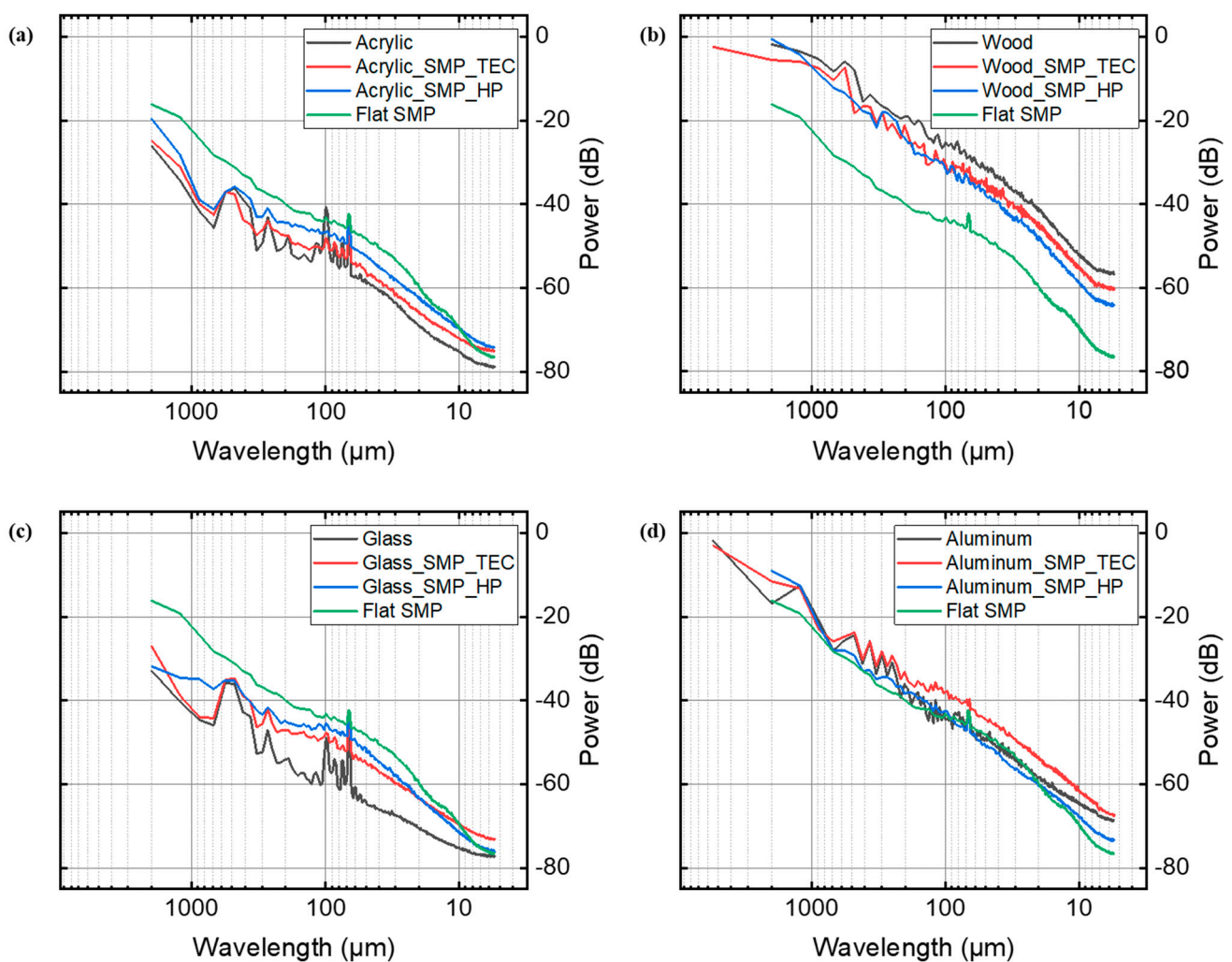


Figure 11. Radially averaged Fourier power spectrum data from 2-dimensional raw roughness height data for different adherend materials including acrylic (a), wood (b), glass (c), and aluminum (d). The black line indicates the spectrum of the target adherend. The red and blue lines individually indicate the spectra of the SMP that has shape adapted to the target adherend using the thermoelectric Peltier module (TEC) and hotplate (HP), respectively. The green line indicates the spectrum for the flat state of the SMP before adhering which is identical for all (a–d).

6. SMP Adhesive Gripper

6.1. Schematic of an SMP Gripper

The computer-aided design (CAD) model and photograph of the SMP adhesive gripper including three legs and three feet, are shown in Figure 12a. Ball joints with a maximum swivel angle of 35° link the legs and feet. The top link and the bottom links are connected to the middle links by pin-in-slot joints. Machined aluminum and 3D printed parts make up the majority of the body. The three feet are all wired in parallel to a lithium polymer (LiPo) battery with a voltage of 11.1 V and a capacity of 1200 mAh (Kinexsis). Wires between the feet and the gripper's external lead are hidden inside aluminum frames. Three TECs are used for heating and cooling cycles and are located under three feet. A 15 ampere maximum double-pole, double-throw (DPDT) switch with the 'center position off' is used to control the TECs by switching electrical polarity and hence the direction of current flow.

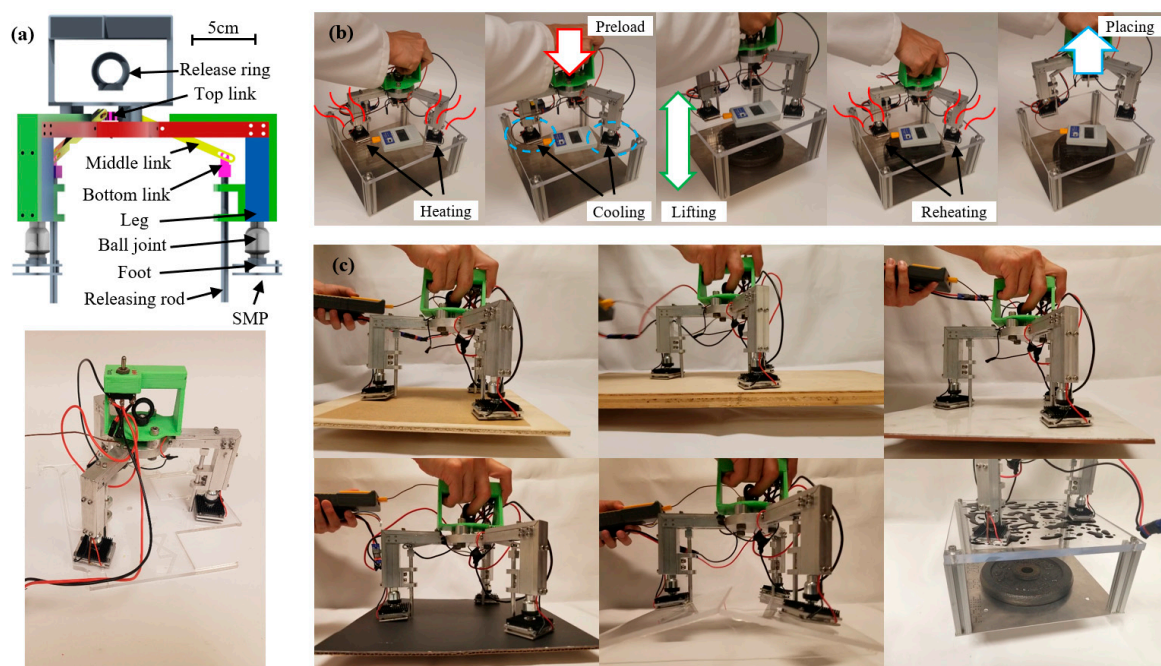


Figure 12. (a) A computer aided design (CAD) drawing and photograph of an SMP adhesive gripper. A battery and thermocouples are included in the gripper for heating/cooling and temperature sensing. (b) The SMP adhesive gripper is used to demonstrate pick-and-place functionality. (c) Images show the SMP adhesive gripper picking up sandpaper, a wooden plate, a tile, poster paper, and an angled acrylic plate, as well as an acrylic plate wet with blue-dyed water.

6.2. Pick-and-Place Procedure

The SMP is heated to a rubbery state during the picking step. The preload is then applied, and the SMP is cooled to a glassy state at the same time. Due to the strong dry adhesion of the SMP, the gripper is bonded to the target object and ready for picking at this point. During the placing step, the SMP is heated again to the rubbery state which is the weak adhesion state. A releasing force is applied to peel the SMP with the operator's manipulation, and the gripper is able to place the target object.

6.3. SMP Gripper Demonstration

A pick-and-place demonstration of a one-hand-operated SMP adhesive gripper is performed on a custom built 30 cm × 30 cm × 14 cm stage with an acrylic plate top. Figure 12b depicts the overall pick-and-place step in which the SMP is first heated to over 90°C , preloaded, and then cooled to 40°C at the same time. Afterwards, the SMP gripper

picks up the stage with a 4.5 kg weight added. Finally, the SMP is reheated over 90 °C, and a releasing force is applied to place the weight. See Video S1 for a demonstration video.

The SMP used in this study is also capable of adhering to wet, non-flat, or moderately rough surfaces in addition to dry, flat, and smooth surfaces. Figure 12c shows those surfaces which are picked up by the SMP adhesive gripper. The video for various surface pick-and-place demonstration can be found in Videos S2 and S3. These results show the pick-up capabilities of the SMP gripper. In Figure 13, optical images and surface roughness profiles of sandpaper, wood, tile, poster paper, and acrylic plate surfaces shown in Figure 12c are acquired using a Keyence VK-X1000 3D laser scanning confocal microscope. The arithmetic average roughness (Ra) magnitudes of the surfaces are 14.1 μm (sandpaper), 6.58 μm (wood), 0.267 μm (tile), 2.04 μm (poster paper), and 0.983 μm (acrylic plate), respectively. The demonstration here provides some insights on the integration of an SMP adhesive into a dry adhesive gripper and its potential to use in a practical situation.

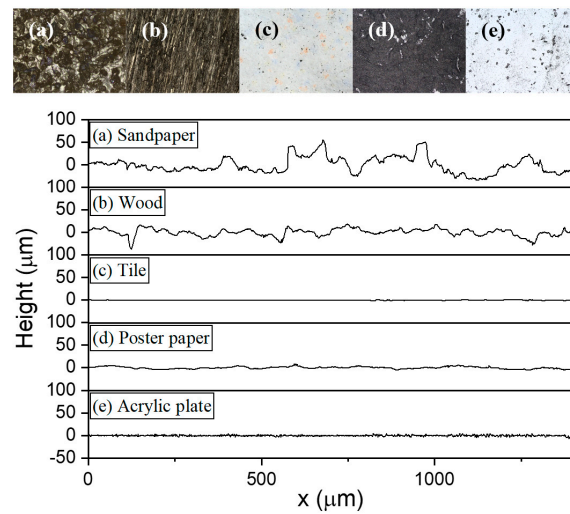


Figure 13. Optical microscope images and surface roughness profiles of (a) sandpaper, (b) a wooden plate, (c) a tile, (d) poster paper, and (e) an acrylic plate used in the picking demonstration.

6.4. Picking Mechanism of the SMP Gripper

An SMP is heated and brought down to a target object in the picking step, and the ball joints between the legs and feet rotate passively to make conformal contact. The step of applying a preload, which is the total of the gripper weight (F_M) and an external force (F_E), is shown in Figure 14a. Because the preload is so important for adhesive performance [51], it is desirable to have a high F_E to meet the inequality below, where P_{pre} is the minimum preload pressure for a reliable adhesive grip, and A is the area of contact.

$$(F_M + F_E) / A > P_{pre} \tag{8}$$

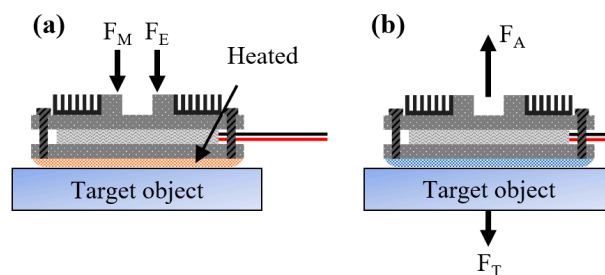


Figure 14. The free body diagram of the foot of an SMP adhesive gripper: (a) forces during preloading; (b) forces during picking.

The SMP bonds to the target object after cooling, allowing the gripper to pick it up. As illustrated in Figure 14b, the weight of the target object (F_T) must not exceed the adhesive force of the SMP (F_A). The adhesion strength of the SMP to a flat and smooth glass plate (P_S) has been previously measured at 5–30 N/cm² [58]. As a result, the maximum weight the gripper can carry should be,

$$F_T < F_A = P_S \times A \tag{9}$$

F_T should be less than 240 N if P_S is considered to be 5 N/cm² and less than 1440 N if P_S is supposed to be 30 N/cm² using the magnitude of A in Table 2.

Table 2. Parameters of the SMP adhesive gripper.

Parameter	Symbol	Magnitude
Weight of the device	F_M	12.7 N
Minimum preload pressure	P_{pre}	15 N/cm ² [51]
Total SMP area	A	48 cm ²
Angle between the middle link and the leg	θ	0–33.6°
Length from pivot point O to top link	L_a	25 mm
Length from pivot point O to bottom link	L_b	50 mm
Release ring pulling force	F_H	60 N [59]

6.5. Placing Mechanism of the SMP Gripper

Figure 15a shows a pin-in-slot joint that connects the middle and bottom links, which is also seen in Figure 12a. The linkages do not move after the SMP adhesive gripper has adhered to a target object; hence, a static condition is assumed. The force is applied from the slot to the pin indicated F_P in Figure 15a which can be divided into horizontal and vertical forces, $F_P \sin \theta$ and $F_P \cos \theta$, respectively. The vertical force ($F_P \cos \theta$) is obviously equal to the ground reaction force (F_G), which is labeled in Figure 15b.

$$F_G = F_P \cos \theta \tag{10}$$

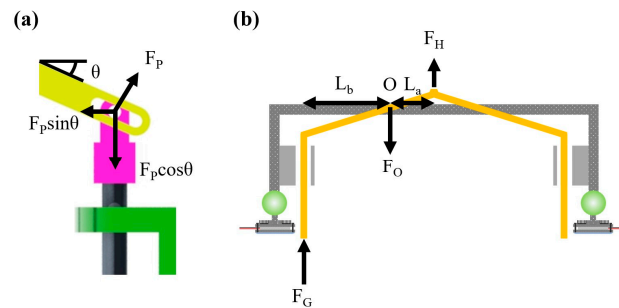


Figure 15. (a) The magnified view of a pin-in-slot joint used between the links; (b) the schematic of a SMP adhesive gripper and the free body diagram of the links.

When placing the target object, large F_G is more desirable since the SMP is easier to be peeled off. By selecting the initial angle of the middle link (θ) as zero, F_G can be maximized according to (10).

The forces acting on the middle link are depicted in Figure 15b. A force imparted to the releasing ring is mechanically transferred to each of the releasing rods via the middle links. The force applied to the release ring is referred to as F_H . Simultaneously, the target object provides a response force F_G . The sum of the moments at the pivot point O should be zero in a static condition,

$$\sum M_O = \frac{F_H}{3} L_a - F_G L_b = 0 \tag{11}$$

The distance between point O and the top or bottom link is indicated as L_a and L_b , respectively. Using (11) in conjunction with L_a and L_b in Table 2, F_G is determined to be 10 N when a typical gripping force F_H of a human is 60 N [59]. In addition, in the static state of the middle link in Figure 15b, the following equation must be met for the force equilibrium:

$$\sum F = \frac{F_H}{3} + F_G - F_O = 0 \quad (12)$$

As a result, 30 N is estimated as the force imparted to the middle link at position O (F_O). Simultaneously, the gripper's leg is subjected to the same force as F_O but in the opposite direction.

6.6. Temperature Analysis

The temperature profile of the SMP adhesive gripper foot, which is heated and cooled with the TEC powered by a three-cell LiPo battery, is measured using a thermocouple. The temperature of the SMP is indicated as the "SMP side", and the temperature of the heat-releasing fin is indicated as the "Fin side" in Figure 16. At 0 s, the switch is turned on to the heating position, and the heat flows from the fin side to the SMP side for the first 30 s. The SMP temperature reaches over 80 °C after 20 s of heating, and the switch is turned into cooling mode between 36 and 52 s which causes the electricity to flow in the other direction. The heat transfers from the SMP side to the fin side in this condition, significantly reducing the cooling time when compared to natural convection cooling. The cooling switch is turned off at the time the SMP side temperature cools down to 40 °C. However, residual heat in the fin side raises the final temperature of the SMP side to 48 °C, which then gradually drops. Because the storage modulus of the SMP actually gradually decreases through T_g rather than a fast transition at T_g , as inferred from Figure 1, sufficient adhesion of the SMP can still be produced even slightly above T_g , such as 40–50 °C.

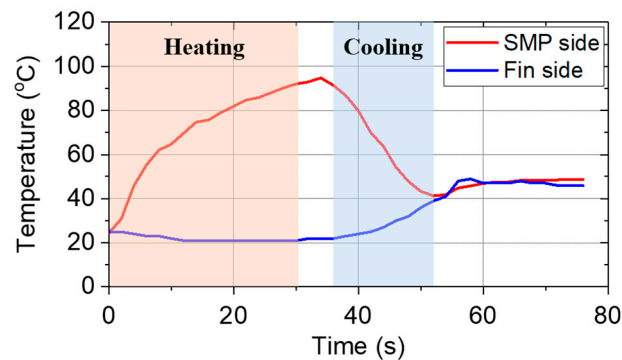


Figure 16. The temperature profile of an SMP adhesive gripper foot during heating and cooling with a TEC as a function of time.

7. Conclusions

A gripper with an SMP adhesive is designed, produced, and tested in this paper. Picking and placing mechanisms are studied in depth in order to enable single-handed operation of the gripper. The dual SMP, which is made up of two stiffness SMPs, is designed to distribute stress more uniformly across the adhesive interface, resulting in delayed contact failure and increased adhesion strength. In addition, the SMP with release tip shows easier detachment by minimizing the adhesion strength due to the increasing stress concentration around the release tip. A bi-layer SMP is more favorable for the adhesive properties required to absorb shock, energy, and dynamic stress when a high static adhesion force is not critically required. Implementing a TEC greatly improves the SMP gripper by increasing the adhesion strength which stems from better conformal contact as proven in RAPSD analysis. In addition, the operation time can be significantly reduced by utilizing the heat flow flexibility of the TEC. This rapid cooling is also advantageous

because it allows for more stable adhesive contact of the SMP against any disturbance, such as operator-contributed vibration, during cooling. These numerical and experimental findings show the SMP adhesive gripper's successful pick-and-place capabilities, as well as the potential of using it for various applications. As future work, we aim to reduce the required time for operation and to extend the experiments to include adhesion gripping tests on porous surfaces.

Supplementary Materials: The following supporting information can be downloaded at: <https://www.mdpi.com/article/10.3390/robotics12020059/s1>, Video S1: Picking and placing demonstration; Video S2: Wet surface demonstration; Video S3: Various surface picking demonstration.

Author Contributions: Conceptualization, C.S.; methodology, C.S.; software, C.S., S.J. and S.L.; validation, C.S., S.J. and S.L.; formal analysis, C.S., S.J. and S.L.; investigation, C.S.; resources, C.S., S.J. and S.L.; data curation, C.S.; writing—original draft preparation, C.S.; writing—review and editing, P.M.F. and S.K.; visualization, C.S.; supervision, P.M.F. and S.K.; project administration, S.K.; funding acquisition, S.K. All authors have read and agreed to the published version of the manuscript.

Funding: This research was funded by the National Science Foundation, grant number ECCS-1950009 and the National Research Foundation of Korea (NRF) funded by Ministry of Science and ICT, grant number 2022M317A3050820; 2022R1A4A3033320; 2022R1A2C3006420.

Data Availability Statement: Data available on request due to restrictions.

Conflicts of Interest: The authors declare no conflict of interest.

References

- Farinelli, A.; Boscolo, N.; Zanutto, E.; Pagello, E. Advanced Approaches for Multi-Robot Coordination in Logistic Scenarios. *Robot. Auton. Syst.* **2017**, *90*, 34–44. [[CrossRef](#)]
- Stoyanov, T.; Vaskevicius, N.; Mueller, C.A.; Fromm, T.; Krug, R.; Tincani, V.; Mojtahedzadeh, R.; Kunaschk, S.; Mortensen Ernits, R.; Canelhas, D.R.; et al. No More Heavy Lifting: Robotic Solutions to the Container Unloading Problem. *IEEE Robot. Autom. Mag.* **2016**, *23*, 94–106. [[CrossRef](#)]
- Jiang, H.; Hawkes, E.W.; Fuller, C.; Estrada, M.A.; Suresh, S.A.; Abcouwer, N.; Han, A.K.; Wang, S.; Ploch, C.J.; Parness, A.; et al. A Robotic Device Using Gecko-Inspired Adhesives Can Grasp and Manipulate Large Objects in Microgravity. *Sci. Robot.* **2017**, *2*, 28. [[CrossRef](#)]
- Parness, A.; Frost, M.; Thatte, N.; King, J.P.; Witkoe, K.; Nevarez, M.; Garrett, M.; Aghazarian, H.; Kennedy, B. Gravity-Independent Rock-Climbing Robot and a Sample Acquisition Tool with Microspine Grippers. *J. Field Robot.* **2013**, *30*, 897–915. [[CrossRef](#)]
- Kuriyama, Y.; Okino, Y.; Wang, Z.; Hirai, S. A Wrapping Gripper for Packaging Chopped and Granular Food Materials. In Proceedings of the 2019 2nd IEEE International Conference on Soft Robotics (RoboSoft), Seoul, Korea, 14–18 April 2019; pp. 114–119. [[CrossRef](#)]
- Wang, Z.; Furuta, H.; Hirai, S.; Kawamura, S. A Scooping-Binding Robotic Gripper for Handling Various Food Products. *Front. Robot. AI* **2021**, *8*, 43. [[CrossRef](#)]
- Wang, Z.; Or, K.; Hirai, S. A Dual-Mode Soft Gripper for Food Packaging. *Rob. Auton. Syst.* **2020**, *125*, 103427. [[CrossRef](#)]
- Lien, T.K. Gripper Technologies for Food Industry Robots. In *Robotics and Automation in the Food Industry Current and Future Technologies*; Woodhead Publishing: Sawston, UK, 2013; pp. 143–170. [[CrossRef](#)]
- Zhang, H.; Kumar, A.S.; Chen, F.; Fuh, J.Y.H.; Wang, M.Y. Topology Optimized Multimaterial Soft Fingers for Applications on Grippers, Rehabilitation, and Artificial Hands. *IEEE/ASME Trans. Mechatron.* **2019**, *24*, 120–131. [[CrossRef](#)]
- Rateni, G.; Cianchetti, M.; Ciuti, G.; Menciasci, A.; Laschi, C. Design and Development of a Soft Robotic Gripper for Manipulation in Minimally Invasive Surgery: A Proof of Concept. *Meccanica* **2015**, *50*, 2855–2863. [[CrossRef](#)]
- Galloway, K.C.; Becker, K.P.; Phillips, B.; Kirby, J.; Licht, S.; Tchernov, D.; Wood, R.J.; Gruber, D.F. Soft Robotic Grippers for Biological Sampling on Deep Reefs. *Soft Robot.* **2016**, *3*, 23–33. [[CrossRef](#)]
- Licht, S.; Collins, E.; Mendes, M.L.; Baxter, C. Stronger at Depth: Jamming Grippers as Deep Sea Sampling Tools. *Soft Robot.* **2017**, *4*, 305–316. [[CrossRef](#)] [[PubMed](#)]
- Cecil, J.; Vasquez, D.; Powell, D. A Review of Gripping and Manipulation Techniques for Micro-Assembly Applications. *Int. J. Prod. Res.* **2007**, *43*, 819–828. [[CrossRef](#)]
- Keum, H.; Yang, Z.; Han, K.; Handler, D.E.; Nguyen, T.N.; Schutt-Aine, J.; Bahl, G.; Kim, S. Microassembly of Heterogeneous Materials Using Transfer Printing and Thermal Processing. *Sci. Rep.* **2016**, *6*, 29925. [[CrossRef](#)] [[PubMed](#)]
- Kim, S. Micro-LEGO for MEMS. *Micromachines* **2019**, *10*, 267. [[CrossRef](#)]
- Becedas, J.; Payo, I.; Feliu, V. Two-Flexible-Fingers Gripper Force Feedback Control System for Its Application as End Effector on a 6-DOF Manipulator. *IEEE Trans. Robot.* **2011**, *27*, 599–615. [[CrossRef](#)]

17. Li, X.; Chen, W.; Lin, W.; Low, K.H. A Variable Stiffness Robotic Gripper Based on Structure-Controlled Principle. *IEEE Trans. Autom. Sci. Eng.* **2018**, *15*, 1104–1113. [[CrossRef](#)]
18. El-Atab, N.; Mishra, R.B.; Al-Modaf, F.; Joharji, L.; Alsharif, A.A.; Alamoudi, H.; Diaz, M.; Qaiser, N.; Hussain, M.M. Soft Actuators for Soft Robotic Applications: A Review. *Adv. Intell. Syst.* **2020**, *2*, 2000128. [[CrossRef](#)]
19. Shintake, J.; Cacucciolo, V.; Floreano, D.; Shea, H. Soft Robotic Grippers. *Adv. Mater.* **2018**, *30*, 1707035. [[CrossRef](#)] [[PubMed](#)]
20. Petković, D.; Pavlović, N.D.; Shamshirband, S.; Anuar, N.B. Development of a New Type of Passively Adaptive Compliant Gripper. *Ind. Rob.* **2013**, *40*, 610–623. [[CrossRef](#)]
21. Ilievski, F.; Mazzeo, A.D.; Shepherd, R.F.; Chen, X.; Whitesides, G.M. Soft Robotics for Chemists. *Angew. Chem.* **2011**, *123*, 1930–1935. [[CrossRef](#)]
22. Do, T.N.; Phan, H.; Nguyen, T.-Q.; Visell, Y.; Do, T.N.; Visell, Y.; Phan, H.; Nguyen, T.-Q. Miniature Soft Electromagnetic Actuators for Robotic Applications. *Adv. Funct. Mater.* **2018**, *28*, 1800244. [[CrossRef](#)]
23. Kofod, G.; Wirges, W.; Paajanen, M.; Bauer, S. Energy Minimization for Self-Organized Structure Formation and Actuation. *Appl. Phys. Lett.* **2007**, *90*, 081916. [[CrossRef](#)]
24. Lau, G.K.; Heng, K.R.; Ahmed, A.S.; Shrestha, M. Dielectric Elastomer Fingers for Versatile Grasping and Nimble Pinching. *Appl. Phys. Lett.* **2017**, *110*, 182906. [[CrossRef](#)]
25. Shian, S.; Bertoldi, K.; Clarke, D.R. Dielectric Elastomer Based “Grippers” for Soft Robotics. *Adv. Mater.* **2015**, *27*, 6814–6819. [[CrossRef](#)] [[PubMed](#)]
26. Zhang, H.; Zhang, J.; Zong, G.; Wang, W.; Liu, R. Sky Cleaner 3. *IEEE Robot. Autom. Mag.* **2006**, *13*, 32–41. [[CrossRef](#)]
27. Miyake, T.; Ishihara, H.; Tomino, T. Vacuum-Based Wet Adhesion System for Wall Climbing Robots -Lubricating Action and Seal Action by the Liquid-. In Proceedings of the 2008 IEEE Int. Conf. Robot. Biomimetics, ROBIO 2008, Bangkok, Thailand, 22–25 February 2009; pp. 1824–1829. [[CrossRef](#)]
28. Shintake, J.; Rosset, S.; Schubert, B.; Floreano, D.; Shea, H. Versatile Soft Grippers with Intrinsic Electroadhesion Based on Multifunctional Polymer Actuators. *Adv. Mater.* **2016**, *28*, 231–238. [[CrossRef](#)]
29. Glick, P.; Suresh, S.A.; Ruffatto, D.; Cutkosky, M.; Tolley, M.T.; Parness, A. A Soft Robotic Gripper with Gecko-Inspired Adhesive. *IEEE Robot. Autom. Lett.* **2018**, *3*, 903–910. [[CrossRef](#)]
30. Hawkes, E.W.; Christensen, D.L.; Han, A.K.; Jiang, H.; Cutkosky, M.R. Grasping without Squeezing: Shear Adhesion Gripper with Fibrillar Thin Film. In Proceedings of the 2015 IEEE International Conference on Robotics and Automation (ICRA), Seattle, WA, USA, 26–30 May 2015; pp. 2305–2312. [[CrossRef](#)]
31. Hawkes, E.W.; Jiang, H.; Cutkosky, M.R. Three-Dimensional Dynamic Surface Grasping with Dry Adhesion. *Int. J. Rob. Res.* **2016**, *35*, 943–958. [[CrossRef](#)]
32. Song, S.; Drotlef, D.M.; Majidi, C.; Sitti, M. Controllable Load Sharing for Soft Adhesive Interfaces on Three-Dimensional Surfaces. *Proc. Natl. Acad. Sci. USA* **2017**, *114*, E4344–E4353. [[CrossRef](#)]
33. Song, S.; Sitti, M. Soft Grippers Using Micro-Fibrillar Adhesives for Transfer Printing. *Adv. Mater.* **2014**, *26*, 4901–4906. [[CrossRef](#)]
34. Hu, Q.; Dong, E.; Sun, D. Soft Gripper Design Based on the Integration of Flat Dry Adhesive, Soft Actuator, and Microspine. *IEEE Trans. Robot.* **2021**, *37*, 1065–1080. [[CrossRef](#)]
35. Hao, Y.; Biswas, S.; Hawkes, E.W.; Wang, T.; Zhu, M.; Wen, L.; Visell, Y. A Multimodal, Enveloping Soft Gripper: Shape Conformation, Bioinspired Adhesion, and Expansion-Driven Suction. *IEEE Trans. Robot.* **2021**, *37*, 350–362. [[CrossRef](#)]
36. Liu, C.; Qin, H.; Mather, P.T. Review of Progress in Shape-Memory Polymers. *J. Mater. Chem.* **2007**, *17*, 1543–1558. [[CrossRef](#)]
37. Mohd Jani, J.; Leary, M.; Subic, A.; Gibson, M.A. A Review of Shape Memory Alloy Research, Applications and Opportunities. *Mater. Des.* **2014**, *56*, 1078–1113. [[CrossRef](#)]
38. McCoul, D.; Rosset, S.; Besse, N.; Shea, H. Multifunctional Shape Memory Electrodes for Dielectric Elastomer Actuators Enabling High Holding Force and Low-Voltage Multisegment Addressing. *Smart Mater. Struct.* **2017**, *26*, 025015. [[CrossRef](#)]
39. Wang, W.; Ahn, S.H. Shape Memory Alloy-Based Soft Gripper with Variable Stiffness for Compliant and Effective Grasping. *Soft Robot.* **2017**, *4*, 379–389. [[CrossRef](#)] [[PubMed](#)]
40. Lee, J.H.; Chung, Y.S.; Rodrigue, H. Long Shape Memory Alloy Tendon-Based Soft Robotic Actuators and Implementation as a Soft Gripper. *Sci. Rep.* **2019**, *9*, 11251. [[CrossRef](#)]
41. Xing, S.; Wang, P.; Liu, S.; Xu, Y.; Zheng, R.; Deng, Z.; Peng, Z.; Li, J.; Wu, Y.; Liu, L. A Shape-Memory Soft Actuator Integrated with Reversible Electric/Moisture Actuating and Strain Sensing. *Compos. Sci. Technol.* **2020**, *193*, 108133. [[CrossRef](#)]
42. Li, W.; Liu, Y.; Leng, J. Light-Actuated Reversible Shape Memory Effect of a Polymer Composite. *Compos. Part A Appl. Sci. Manuf.* **2018**, *110*, 70–75. [[CrossRef](#)]
43. Xu, Z.; Ding, C.; Wei, D.W.; Bao, R.Y.; Ke, K.; Liu, Z.; Yang, M.B.; Yang, W. Electro and Light-Active Actuators Based on Reversible Shape-Memory Polymer Composites with Segregated Conductive Networks. *ACS Appl. Mater. Interfaces* **2019**, *11*, 30332–30340. [[CrossRef](#)]
44. Linghu, C.; Zhang, S.; Wang, C.; Yu, K.; Li, C.; Zeng, Y.; Zhu, H.; Jin, X.; You, Z.; Song, J. Universal SMP Gripper with Massive and Selective Capabilities for Multiscaled, Arbitrarily Shaped Objects. *Sci. Adv.* **2020**, *6*, eaay5120. [[CrossRef](#)]
45. Brown, E.; Rodenberg, N.; Amend, J.; Mozeika, A.; Steltz, E.; Zakin, M.R.; Lipson, H.; Jaeger, H.M. Universal Robotic Gripper Based on the Jamming of Granular Material. *Proc. Natl. Acad. Sci. USA* **2010**, *107*, 18809–18814. [[CrossRef](#)]
46. Li, L.; Liu, Z.; Zhou, M.; Li, X.; Meng, Y.; Tian, Y. Flexible Adhesion Control by Modulating Backing Stiffness Based on Jamming of Granular Materials. *Smart Mater. Struct.* **2019**, *28*, 115023. [[CrossRef](#)]

47. Zhu, T.; Yang, H.; Zhang, W. A Spherical Self-Adaptive Gripper with Shrinking of an Elastic Membrane. In Proceedings of the 2016 International Conference on Advanced Robotics and Mechatronics (ICARM), Macau, China, 18–20 August 2016; pp. 512–517. [[CrossRef](#)]
48. Son, C.H.; Kim, S. A Shape Memory Polymer Adhesive Gripper for Pick-and-Place Applications. In Proceedings of the Proceedings-IEEE International Conference on Robotics and Automation, Paris, France, 15 September 2020; pp. 10010–10016.
49. Park, J.K.; Eisenhaure, J.D.; Kim, S. Reversible Underwater Dry Adhesion of a Shape Memory Polymer. *Adv. Mater. Interfaces* **2019**, *6*, 1801542. [[CrossRef](#)]
50. Eisenhaure, J.; Kim, S. High-Strain Shape Memory Polymers as Practical Dry Adhesives. *Int. J. Adhes. Adhes.* **2018**, *81*, 74–78. [[CrossRef](#)]
51. Eisenhaure, J.D.; Rhee, S., II; Al-Okaily, A.M.; Carlson, A.; Ferreira, P.M.; Kim, S. The Use of Shape Memory Polymers for MEMS Assembly. *J. Microelectromechan. Syst.* **2016**, *25*, 69–77. [[CrossRef](#)]
52. Seo, J.; Eisenhaure, J.; Kim, S. Micro-Wedge Array Surface of a Shape Memory Polymer as a Reversible Dry Adhesive. *Extrem. Mech. Lett.* **2016**, *9*, 207–214. [[CrossRef](#)]
53. Patil, S.; Malasi, A.; Majumder, A.; Ghatak, A.; Sharma, A. Reusable Antifouling Viscoelastic Adhesive with an Elastic Skin. *Langmuir* **2011**, *28*, 42–46. [[CrossRef](#)]
54. Shahsavan, H.; Zhao, B. Bioinspired Functionally Graded Adhesive Materials: Synergetic Interplay of Top Viscous-Elastic Layers with Base Micropillars. *Macromolecules* **2014**, *47*, 353–364. [[CrossRef](#)]
55. Dharmawan, A.G.; Xavier, P.; Hariri, H.H.; Soh, G.S.; Baji, A.; Bouffanais, R.; Foong, S.; Low, H.Y.; Wood, K.L. Design, Modeling, and Experimentation of a Bio-Inspired Miniature Climbing Robot With Bilayer Dry Adhesives. *J. Mech. Robot.* **2019**, *11*, 020902. [[CrossRef](#)]
56. Minsky, H.K.; Turner, K.T. Composite Microposts with High Dry Adhesion Strength. *ACS Appl. Mater. Interfaces* **2017**, *9*, 18322–18327. [[CrossRef](#)]
57. Dong, W.P.; Stout, K.J. Two-Dimensional Fast Fourier Transform and Power Spectrum for Surface Roughness in Three Dimensions. *Proc. Inst. Mech. Eng. Part B J. Eng. Manuf.* **1995**, *209*, 381–391. [[CrossRef](#)]
58. Eisenhaure, J.; Kim, S. An Internally Heated Shape Memory Polymer Dry Adhesive. *Polymers* **2014**, *6*, 2274–2286. [[CrossRef](#)]
59. Astin, A.D. *Finger Force Capability: Measurement and Prediction Using Anthropometric and Myoelectric Measures*; Virginia Tech: Blacksburg, VA, USA, 1999.

Disclaimer/Publisher’s Note: The statements, opinions and data contained in all publications are solely those of the individual author(s) and contributor(s) and not of MDPI and/or the editor(s). MDPI and/or the editor(s) disclaim responsibility for any injury to people or property resulting from any ideas, methods, instructions or products referred to in the content.